Progress In Electromagnetics Research, PIER 97, 105–127, 2009

ANALYSIS OF SCATTERING FROM ARBITRARY CONFIGURATION OF CYLINDRICAL OBJECTS USING HYBRID FINITE-DIFFERENCE MODE-MATCHING METHOD

A. Kusiek and J. Mazur

Faculty of Electronics, Telecommunications and Informatics
Department of Microwave and Antenna Engineering
Gdansk University of Technology
11/12 Gabriela Narutowicza Street, 80-233 Gdansk, Poland

Abstract—This paper presents a new hybrid finite-difference frequency domain — mode-matching method (FDFD-MM) for the analysis of electromagnetic wave scattering from configuration of metallic or dielectric cylindrical posts with arbitrary cross-section. In our approach each scatterer is treated as an effective circular cylinder represented by impedance matrix defined in its local coordinate system. In order to obtain the scattering parameters of arbitrary configuration of objects in global coordinate system an analytical iterative scattering procedure (ISP) is applied. This work is an extension of our previously published results, where our consideration were limited to two dimensional (2D) problems with TM excitation. In this paper, we extended our analysis to two-and-a-half dimensional (2.5D) problems. The accuracy of the proposed method is presented and discussed. To verify our approach some numerical examples are presented. The obtained results are compared with the results published in literature and the ones obtained from own measurements and commercial software.

1. INTRODUCTION

The rapid increase of interest in wireless communication systems requires developing of new microwave components. One group of these components are the structures where cylindrical posts of arbitrary shape are applied to obtain desired scattering parameters [1–12]. Generally, in the analysis of these components open and closed

Corresponding author: A. Kusiek (adakus@eclipse.eti.pg.gda.pl).

problems can be distinguished. In the open problems, the near or far scattered field pattern of a set of cylindrical objects located in free space and illuminated with plane wave or Gaussian beam is the subject of interest. These structures are applied to the reduction of strut radiation of reflector antennas [1, 2], novel EBG structures realized as periodical arrays [3, 4] and polarizers [5, 6]. In the closed problems the result of the analysis are scattering parameters of waveguide junctions or resonant frequencies of resonators loaded with cylindrical objects. Rectangular waveguide junctions and circular cavities consisting of single or multiple cylindrical posts are applied to filters [7, 8], resonators [9], phase shifters [10], polarizers [11], multiplexers or power dividers [12].

Since, in considered problems objects with arbitrary shape are assumed, the most powerful techniques of analysis are hybrid methods [13–21]. In these method the discrete techniques such as finite element method (FEM) [13–15], finite-difference time domain method (FDTD) [16–18] or frequency domain (FDFD) [19] methods and method of moments (MoM) [18, 20, 21] are used in limited region surrounding the analyzed structure. In the outer region the fields are combined with analytical solution of the problem using e.g., integral equation technique [15, 17] for open structures or general scattering matrix (GSM) approach for closed problems [13, 20, 21]. As a result, the hybrid techniques allows one to achieve higher flexibility, increase the accuracy and reduce the numerical complexity of the analysis.

In this paper a novel hybrid method is proposed which combines the finite difference frequency domain method with analytical mode-matching technique (FDFD-MM). In comparison to alternative methods [13–21] the presented approach allows one to analyze scattering from arbitrary set of cylindrical objects which can be located both in free space or in waveguide junctions. At first, in our approach each single object is considered separately in its local coordinate system. The proposed hybrid technique is used to determine the impedance matrix which defines a relation between electric and magnetic tangential field components on artificial cylindrical surface surrounding analyzed object. Since, the impedance matrix of each scatterer is known, the analytical iterative scattering procedure can be applied to determine the scattering parameters of arbitrary configuration of objects [22, 23]. Presented analysis is an extension of our work presented in [24] where the analysis was limited to two dimensional problems with TM excitation. In this paper the method is extended to two-and-a-half dimensional (2.5D) problems. The accuracy of the method is verified and discussed. The presented numerical results are compared with analytical results published in

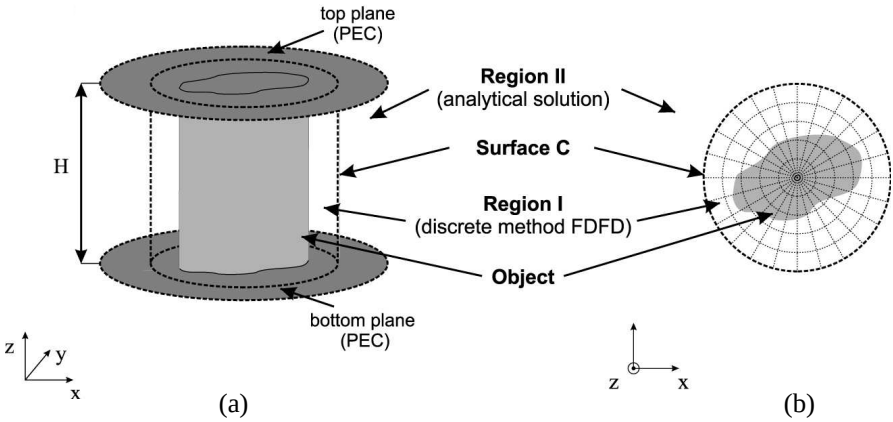

Figure 1. Single post analysis in local coordinate system, (a) 3D view of the structure, (b) cross-section of the structure.

literature and the results obtained from own measurements and commercial software QuickWave 3D [25].

2. FORMULATION OF THE PROBLEM

2.1. Single Object

We start our analysis from a single object in its local coordinate system (see Fig. 1). In our approach we introduce lateral surface $\mathcal{C}$:

$$\mathcal{C} : \begin{cases} \rho = R, \\ \varphi \in [0, 2\pi], \\ z \in [0,\ H], \end{cases} \tag{1}$$

which surrounds analyzed object and divides the computation domain into two regions, where analytical (Region II) and discrete FDFD (Region I) solution of Maxwell equations are used, respectively. In Region II the z components of electric and magnetic fields are expressed as follows:

$$E_z^{II}(\rho, \varphi, z) = \sum_{k=1}^{2} \sum_{n=0}^{N} \sum_{m=-M}^{M} A_{knm}^{e} R_m^k(k_{\rho n}\rho) f_{nm}^{e}(\varphi, z), \tag{2}$$

$$H_z^{II}(\rho, \varphi, z) = \sum_{k=1}^{2} \sum_{n=1}^{N} \sum_{m=-M}^{M} A_{knm}^{h} R_m^k(k_{\rho n}\rho) f_{nm}^{h}(\varphi, z), \tag{3}$$

where

$$f^e_{nm}(\varphi, z) = e^{im\varphi}\cos(k_{zn}z), \tag{4}$$
$$f^h_{nm}(\varphi, z) = e^{im\varphi}\sin(k_{zn}z) \tag{5}$$

and: $k_{zn} = n\pi/H$, $k_{\rho n} = \sqrt{(k_0)^2 - (k_{zn})^2}$, $k_0 = 2\pi f/c$, $R^1_m(\cdot)$ and $R^2_m(\cdot)$ are Bessel and Hankel function of the second kind and mth order, respectively and $A^{e,h}_{knm}$ are unknown expansion coefficients. The φ components of electric and magnetic fields can be found using the following relations:

$$E_\varphi = \frac{1}{k^2_{\rho n}}\left(i\omega\mu_0\frac{\partial H_z}{\partial\rho} + \frac{1}{\rho}\frac{\partial^2 E_z}{\partial\varphi\partial z}\right), \tag{6}$$

$$H_\varphi = \frac{1}{k^2_{\rho n}}\left(-i\omega\varepsilon_0\frac{\partial E_z}{\partial\rho} + \frac{1}{\rho}\frac{\partial^2 H_z}{\partial\varphi\partial z}\right). \tag{7}$$

In the inner region (see Fig. 1) the tangential components of electric and magnetic fields defined on lateral surface $\mathcal{C}$ can be expressed as follows:

$$E^I_z(R, \varphi, z) = \sum_{n=0}^{N}\sum_{m=-M}^{M} C^{Ez}_{nm} f^e_{nm}(\varphi, z), \tag{8}$$

$$H^I_z(R, \varphi, z) = \sum_{n=1}^{N}\sum_{m=-M}^{M} D^{Hz}_{nm} f^h_{nm}(\varphi, z), \tag{9}$$

$$E^I_\varphi(R, \varphi, z) = \sum_{n=1}^{N}\sum_{m=-M}^{M} C^{E\varphi}_{nm} f^h_{nm}(\varphi, z), \tag{10}$$

$$H^I_\varphi(R, \varphi, z) = \sum_{n=0}^{N}\sum_{m=-M}^{M} D^{H\varphi}_{nm} f^e_{nm}(\varphi, z), \tag{11}$$

where C^{Ez}_{nm}, $C^{E\varphi}_{nm}$, D^{Hz}_{nm} and $D^{H\varphi}_{nm}$ are unknown expansion coefficients of electric and magnetic fields.

Now, by imposing the boundary continuity conditions on surface $\mathcal{C}$ between tangential components of electric and magnetic fields defined in Regions I and II the following set of equations is obtained:

$$\begin{aligned} E^{II}_z(R, \varphi, z) &= E^I_z(R, \varphi, z), \\ E^{II}_\varphi(R, \varphi, z) &= E^I_\varphi(R, \varphi, z), \\ H^{II}_z(R, \varphi, z) &= H^I_z(R, \varphi, z), \\ H^{II}_\varphi(R, \varphi, z) &= H^I_\varphi(R, \varphi, z), \end{aligned} \tag{12}$$

where $\varphi \in [0, 2\pi]$, $z \in [0, H]$. Taking the advantage of orthogonality of f^e_{nm} and f^h_{nm} set of Eq. (12) can be rewritten in the matrix form as follows:

$$\mathbf{M}_1^E \mathbf{A}_1 + \mathbf{M}_2^E \mathbf{A}_2 = \mathbf{C}, \tag{13}$$

$$\mathbf{M}_1^H \mathbf{A}_1 + \mathbf{M}_2^H \mathbf{A}_2 = \mathbf{D} \tag{14}$$

where all matrices are defined in Appendix A. Let us now introduce the impedance **Z**-matrix representation of the object:

$$\mathbf{C} = \mathbf{Z}\mathbf{D} \tag{15}$$

which defines the relation between the expansion coefficients **C** and **D** of tangential electric (8), (10) and magnetic (9), (11) fields, respectively. In order to determine the **Z**-matrix representation of the object, the discrete FDFD technique is used (see 2.2). Since, the **Z**-matrix of the object is known, it can be utilized to determine a more convenient representation of the object in a form of **T**-matrix:

$$\mathbf{A}_2 = \mathbf{T}\mathbf{A}_1 \tag{16}$$

which defines the relation between incident $\mathbf{A_1}$ and scattered $\mathbf{A_2}$ field coefficients. It must be emphasized that **T**-matrix depends on the geometry and material properties of the object but not on the excitation. This approach allows us to limit our consideration to Region II where the scatterer is treated as an effective circular cylinder described by its **T**-matrix. For such an effective cylinder the scattered field can be found for any incident wave. Since the **T**-matrix is determined, a rotation of the object by any angle φ_0 can be obtained as follows:

$$\boldsymbol{T}_{(\varphi=\varphi_0)} = \boldsymbol{R}_t \, \boldsymbol{T}_{(\varphi=0)} \, \boldsymbol{R}_t^* \tag{17}$$

where $\boldsymbol{R} = \mathrm{diag}(\mathbf{R}_1, \ldots, \mathbf{R}_{2N+1})$ and $\boldsymbol{R}_i = \mathrm{diag}(e^{-jM\varphi_0}, \ldots, e^{jM\varphi_0})$.

2.2. Z-Matrix

In order to find the **Z**-matrix relation between tangential electric and magnetic field components on surface $\mathcal{C}$ for arbitrary geometry of structure, the FDFD technique is applied. In this case Region I is discretized in $\rho\varphi$ plane with Yee-mesh, defined in a cylindrical coordinate system (see Fig. 2) with $W = V \times K$ cells where V and K are numbers of cells in ρ and φ direction, respectively. In the z-direction the analytical form of electric and magnetic field variation

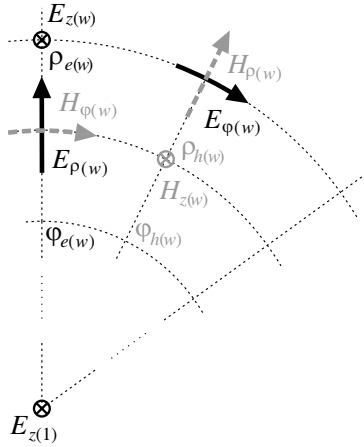

Figure 2. The discrete field components in the wth cell ($w = 1, \ldots, W$).

defined by (4) and (5) is assumed. Now, Maxwell equations can be written in a discrete form [26] as follows:

$$\mathbf{P}_1\mathbf{D}_1(\mathbf{Q}\mathbf{E} + \mathbf{Q}_b\mathbf{E}_b) = j\omega\mu_0\mathbf{S}_1\mathbf{H}, \tag{18}$$

$$\mathbf{P}_2\mathbf{D}_2\mathbf{H} = j\omega\varepsilon_0\varepsilon_r\mathbf{S}_2\mathbf{E} \tag{19}$$

where $\mathbf{E}_b = [E_{b\varphi(1)}, \ldots, E_{b\varphi(K)}, E_{bz(1)}, \ldots, E_{bz(K)}]^T$ are the probes of tangential field components at surface $\mathcal{C}$ determined by (8) and (10) as follows: $E_{b\varphi(w)} = E^I_\varphi(R, \varphi_{h(w)})$, $E_{bz(w)} = E^I_z(R, \varphi_{e(w)})$ and $\mathbf{E}$ and $\mathbf{H}$ are the vectors of field component probes in the interior area of surface $\mathcal{C}$. For brevity's sake, all the mentioned matrices in above equations are defined in Appendix B. Simple algebraic manipulations using (18) and (19) allow one to find the relation for $\mathbf{H}$ with respect to $\mathbf{E}_b$

$$\mathbf{H} = -j\omega\varepsilon_0\mathbf{G}^{-1}\mathbf{S}_1^{-1}\mathbf{P}_1\mathbf{D}_1\mathbf{Q}_b\mathbf{E}_b \tag{20}$$

where $\mathbf{G} = (\mathbf{S}_1^{-1}\mathbf{P}_1\mathbf{D}_1\mathbf{Q}\varepsilon_r^{-1}\mathbf{S}_2^{-1}\mathbf{P}_2\mathbf{D}_2 + \omega^2\mu_0\varepsilon_0\mathbf{I})$. Using the orthogonality of $f^{e(h)}_{nm}$, and taking each term of (8) and (10) as a boundry condition with arbitrary values of $C^{Ez,\varphi}_{nm}$, separately the unknown $D^{Hz,\varphi}_{knm}$ coefficients of magnetic field components expressed on contour $\mathcal{C}$ as

$$H^{nm}_{z,\varphi}(\rho = R, \varphi) = \sum_{k=-M}^{M} D^{Hz,\varphi}_{knm} f^{h,e}_{kn}(\varphi, z), \tag{21}$$

are obtained. Now, utilizing coefficients $C_{nm}^{Ez,\varphi}$ and $D_{knm}^{Hz,\varphi}$ the **Z**-matrix (15) can be obtained as follows:

$$\mathbf{Z} = \left(\mathbf{D}^{\mathbf{H}}\right)^{-1} \mathbf{C}^{\mathbf{E}}, \tag{22}$$

where matrices $\mathbf{C}^E$ and $\mathbf{D}^H$ are defined in Appendix B.

To improve the accuracy of FDFD solution the approximation methods of the object shape with arbitrary geometry in Yee mesh are used. In the case of metallic objects the conformal mesh method is used [27]. In this method the shape of mesh cells on the surface of the metal is modified to fit the geometry of the object and Maxwell equations (18) and (19) are updated accordingly. In the case of dielectric objects the effective dielectric constant algorithm [28] modified to cylindrical coordinate system [29] is applied. In this algorithm for the mesh cells containing boundaries between regions with two different values of dielectric constants ($\varepsilon_1 \neq \varepsilon_2$) the effective dielectric constants are computed and these values are next used to update the ε_r matrix.

2.3. Multiple Object Scattering

In order to find the **T**-matrix of the arbitrary configuration of objects, the iterative scattering procedure (ISP) thoroughly described in [22, 23] can be applied. The ISP is based on the interaction of the individual posts and allows to find the total scattered field from all the obstacles on a boundary of fixed cylindrical region. During the iterative process the interactions between cylindrical objects are considered. In each iteration the scattered field from each object is treated as an incident field on the other cylinders. When the steady state is achieved

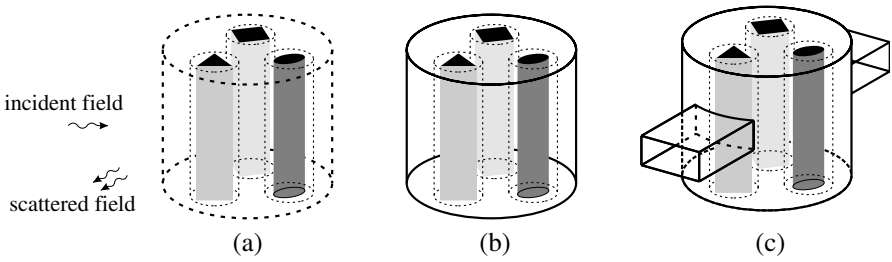

Figure 3. Applications of the proposed method: (a) Plane wave scattering from set of cylindrical objects, (b) loaded circular cavity resonators, (c) loaded circular cavity resonator coupled with rectangular waveguides.

the total scattered field is obtained which can be matched with the outer arbitrary excitation. The outer region can be assumed as an open space with an arbitrary incident wave (see Fig. 3(a)). Since the homogenous along z-axis cylindrical objects are assumed in the analysism functions (4) and (5) take the following form $f_{nm}^{e,h}(\cdot) = e^{im\varphi}e^{ik_z\varphi}$, where $k_z = k_0\sin(\theta_0)$ and θ_0 is the angle of plane wave incidence (see Fig. 4) and the n-related summation in (2), (3) and (8)–(11) is no longer needed. For the closed problems the proposed method can be used to determine resonance frequencies of loaded with set of cylindrical posts circular cavity resonators (Fig. 3(b)) or scattering

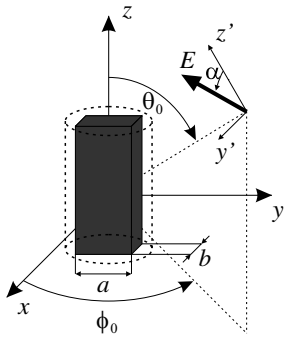

(a)

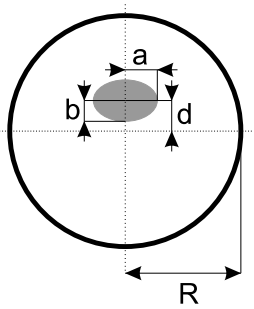

(c)

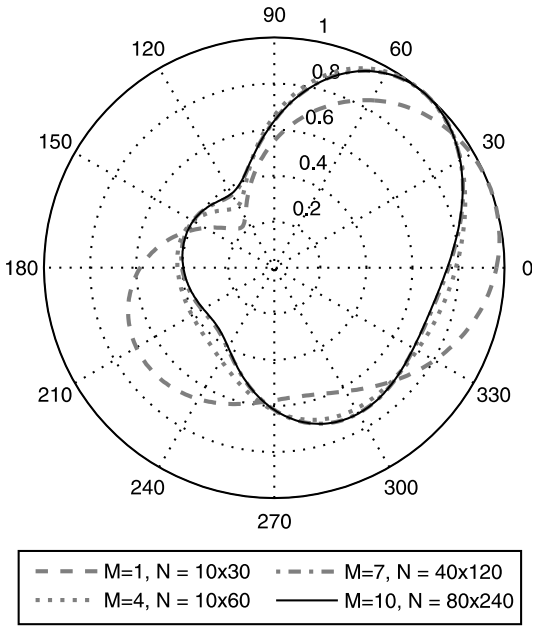

(b)

Figure 4. Convergence analysis: (a) inhomogeneous rectangular metallic cylinder illuminated with plane wave, (b) normalized scattered E_z electric field component pattern for the structure from Fig. 4(a) for different values of number of modes M and mesh density N, (c) circular cavity resonator loaded with asymmetrically located elliptic dielectric cylinder.

parameters of circular resonators coupled with rectangular waveguides (Fig. 3(c)) [22, 23].

3. ACCURACY OF THE METHOD

In order to check the convergence of the presented approach two numerical examples depicted in Fig. 4 will be considered. The first analyzed structure, schematically presented in Fig. 4(a) is a rectangular metallic cylinder illuminated with a plane wave with the following parameters: Direction of incidence $\theta_0 = 30^\circ$ and $\phi_0 = 45^\circ$ and polarization angle $\alpha = 45^\circ$. The scattering patterns of this structure for different values of mesh density W and number of eigenfunctions M are presented in Fig. 4(b). The convergence of the proposed method is verified using the following error criterion

$$\delta_F = \frac{1}{K} \sum_{k=0}^{K} \frac{\left|F_z^W(\varphi_k)\right| - \left|F_z^{RA}(\varphi_k)\right|}{\left|F_z^{RA}(\varphi_k)\right|} \cdot 100\%, \tag{23}$$

where F_z^W is a scattering characteristic of the electric field for the assumed value of W and F_z^{RA} is an asymptotic scattering characteristic of the z-component of electric field obtained from Richardson Approximation (RA) [30]. The obtained results collected in Table 1 show that the accuracy of the method is improved with the increase of both, the mesh density W and the number of cylindrical functions M. It can be seen that the choice of the number of cells $W = 80 \times 240$ and the number of eigenfunctions $M = 10$ allows one to achieve the accuracy better than 0.1%.

Table 1. Absolute value of percentage error δ_F of scattering pattern computation for structure from Fig. 4(a) ($a = 1.2\lambda_0$, $b = 0.4\lambda_0$).

	Mesh density ($W = V \times K$)			
	10×30	20×60	40×120	80×240
$M = 1$	1.87	1.38	1.16	1.04
$M = 2$	3.75	1.83	1.16	0.78
$M = 4$	1.36	0.20	0.07	0.26
$M = 7$	1.72	0.51	0.22	0.03
$M = 10$	1.72	0.54	0.25	0.06

Table 2. Absolute value of percentage error δ_F of resonance frequencies computation for structure from Fig. 4(c) ($a = 8\,\text{mm}$, $b = 2\,\text{mm}$, $d = 0\,\text{mm}$, $R = 20\,\text{mm}$, $H = 50\,\text{mm}$).

Mode	M	Mesh density ($W = I \times J$)			Analytical	Err [%]
		10×30	20×60	40×120		
TM	2	4.5236	4.5033	4.4977	4.4964	0.05
	4	4.5234	4.5031	4.4977		0.05
	7	4.5234	4.5031	4.4976		0.05
	10	4.5234	4.5031	4.4976		0.05
hybrid	2	4.7974	4.8011	4.8022	4.8209	0.39
	4	4.8065	4.8122	4.8141		0.14
	7	4.8088	4.8152	4.8176		0.07
	10	4.809	4.8154	4.8179		0.06
hybrid	2	5.0964	5.1101	5.1159	5.1231	0.14
	4	5.0984	5.1121	5.1178		0.10
	7	5.099	5.1127	5.1184		0.09
	10	5.0991	5.1127	5.1184		0.09

The second example concerns a circular cavity resonator loaded with elliptical dielectric ($\varepsilon_r = 5$) post (see Fig. 4(c)). The convergence of the resonant frequencies of this resonator to the ones obtained from analytical model [31] is presented in Table 2. As in the previous case, the improvement of method accuracy is obtained both with the increasing of mesh density W and number of cylindrical functions M. The convergence of resonant frequencies obtained from our model to the analytical ones is observed. For the mesh density $W = 40 \times 120$ and $M = 10$ the accuracy is higher then 0.1%.

It should be emphasized, that in presented approach the accuracy of the method strongly depends on the analyzed geometry of an object and its material properties. Hence, the parameters of analysis for each investigated object need to be determined individually.

4. NUMERICAL RESULTS

4.1. Open Structures

In this section the four examples of open structures illuminated with obliquely incident plane wave are considered. For all the structures the far scattered field is calculated and compared with commercial software and literature. The first two analyzed structures are a strip-loaded circular dielectric cylinders presented in Figs. 5(a) and (b) and excited with TM and TE plane wave, respectively. In the far field calculation $M = 10$ and mesh density $W = 60 \times 180$ were assumed. The obtained results of analysis for different angles of plane wave incidence are compared with the results presented in [32]. A good agreement of presented method with analytical approach is achieved. In next example, schematically presented in Fig. 6 a configuration of four dielectric cylinders excited with TM plane wave is considered. In the analysis $M = 10$ and mesh density $W = 30 \times 90$ and $P = 20$ iterations in ISP was used to obtain a good accuracy. The results for two different angles of post rotation are compared with the ones obtained from commercial software QuickWave (where 59177 mesh cells was used in the analysis) and a good agreement is observed. Moreover, it can be noticed that the inhomogeneous cross-section of objects allows one to tune the scattered field characteristic. For the first configuration of posts the characteristic has one main lobe 6(a). The rotation of the posts causes the formulation of the second main lobe in $\varphi = 90^\circ$ direction (see Fig. 6(b)).

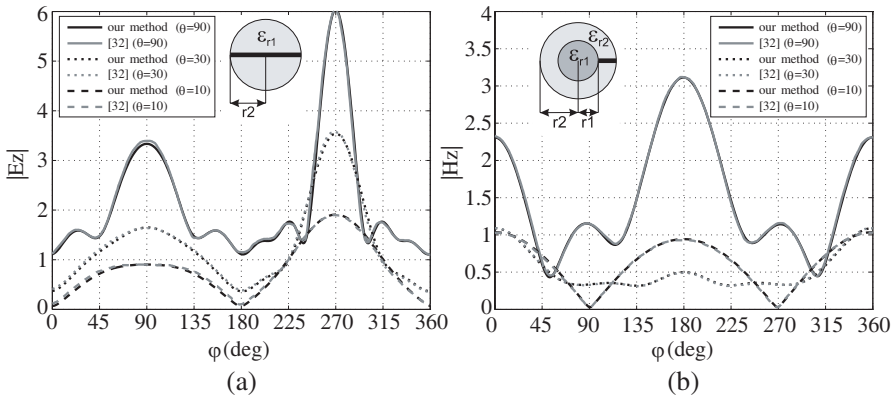

Figure 5. Far-field pattern of the strip loaded dielectric cylinders: (a) $k_0 r = 5$, $\varepsilon_r = 9$ and (b) $k_0 r_1 = 1$, $k_0 r_2 = 2$, $\varepsilon_{r_1} = 5$ and $\varepsilon_{r_2} = 6$ for different angles θ_0 of plane wave incidence ($\phi_0 = \alpha = 0$).

The last example concerns an array of five dielectric circular cylinders loaded with metallic rectangular cylinders and illuminated with TM plane wave (7). In the calculation of far field for above structure the following parameters of the method were assumed $M =$

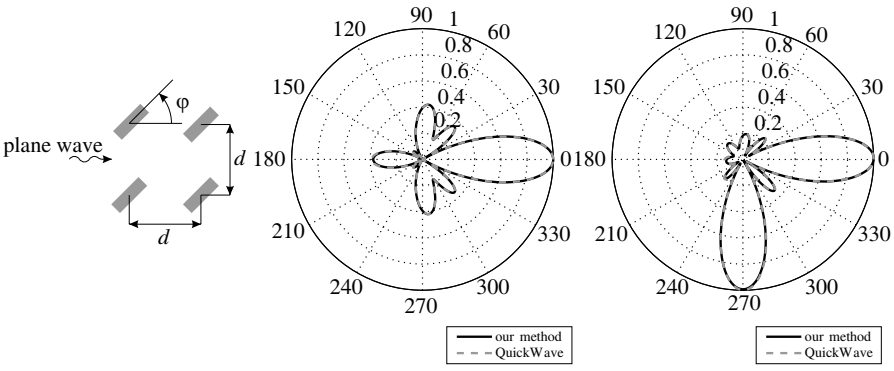

Figure 6. Normalized amplitude of scattered z component of electric field for configuration of four rectangle dielectric posts ($\varepsilon_{ri} = 3$, $a_i = 0.4\lambda_0$, $b_i = 0.1\lambda_0$) illuminated with plane wave ($\alpha = 0$, $\phi_0 = 0$ and $\theta_0 = 90^\circ$) for two angles of post rotations, (a) $\varphi_i = 0$ and (b) $\varphi_i = -45^\circ$ for $i = 1, \ldots, 4$.

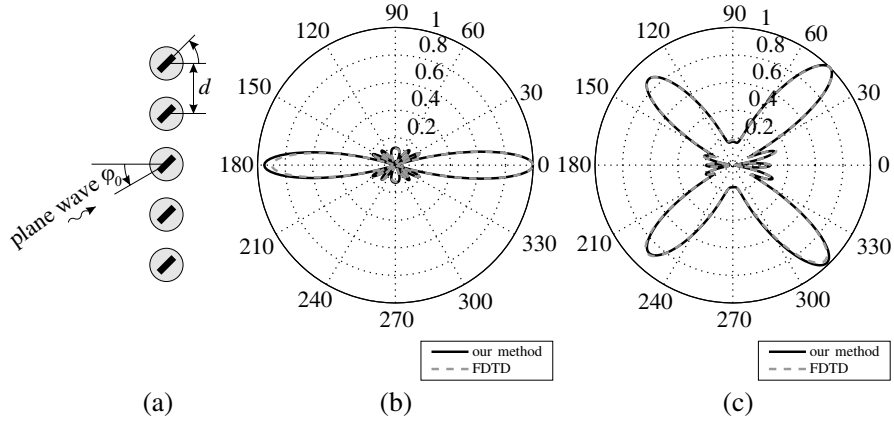

Figure 7. Normalized amplitude of scattered z component of electric field for configuration of five dielectric circular cylinders loaded with rectangle metallic cylinders ($\varepsilon_{ri} = 3$, $r_i = 0.11\lambda_0$, $\varphi_i = 90^\circ$, $a_i = 0.2\lambda_0$, $b_i = 0.04\lambda_0$ for $i = 1, \ldots, 5$) for two different angles ϕ_0 of plane wave illumination ($a = 0$, $\theta_0 = 90^\circ$) (a) $\phi_0 = 0$ and (b) $\phi_0 = 45^\circ$.

10, mesh density $W = 40 \times 120$ and $P = 20$. The results for two different angles ϕ_0 of plane wave illumination are presented in Fig. 7. The obtained results are in good agreement with the ones obtained from QuickWave. From the presented results it can be noticed that the far field pattern is modified by changing the plane wave illumination angle. When the plane wave angle of incidence is changed to $\phi_0 = 45°$ the four main lobe appears in scattered field characteristic.

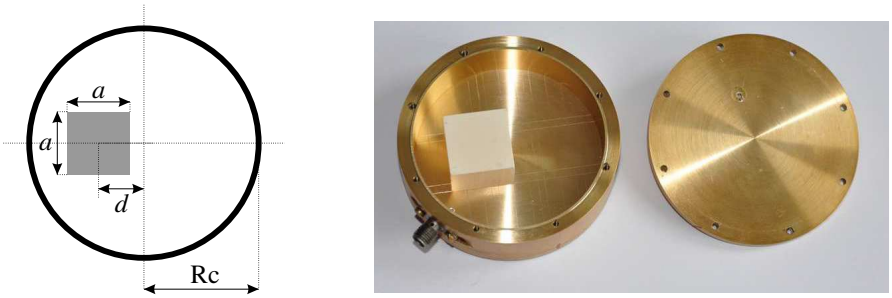

Figure 8. Circular cavity resonator loaded with single square dielectric post: (a) Schematic view, (b) photo of the fabricated structure.

Table 3. TM/TE-modes resonance frequencies (in GHz) of structure from Fig. 8 ($a = 20\,\text{mm}$, $\varepsilon_r = 11.25$, $R_c = 30\,\text{mm}$, $H = 15\,\text{mm}$) or different values of post shift $d\,\text{mm}$.

Mode	n	Our method			Measurement $d = 0$	err [%]
		$d = 15$	$d = 10$	$d = 0$		
TM	0	1.7475	1.6299	1.5553	1.5568	0.10
TM	0	3.2373	3.1275	3.0646	3.0644	0.01
TM	0	3.2969	3.1375			
hybrid	1	4.0254	4.0305	4.0302	4.0056	0.61
hybrid	1	4.0556	4.0343			
TM	0	4.6021	4.4715	4.4229	4.4181	0.11
TM	0	4.7434	4.7523	4.7494	4.75	0.01
hybrid	1	4.8513	4.8222	4.8164	-	-
TM	0	5.1207	5.0591	5.0333	5.0325	0.02
hybrid	1	5.216	5.1927	5.1895	5.17	0.38

4.2. Resonators

In this section, the presented approach is applied to the analysis of circular cavity resonators loaded with arbitrary configuration of dielectric or metallic cylindrical posts. As a result of analysis a resonant frequencies of structures are determined and compared with the results obtained from commercial software QuickWave and own measurements.

As a first example a circular cavity resonator containing a single dielectric post is considered (see Fig. 8). The calculated resonant frequencies of this structure for different post location and measured ones for centrally located square dielectric post are presented in Table 3. In the analysis the number of modes $M = 10$ and mesh density $W = 40 \times 120$ were assumed. It can be noticed that the relative error of measured frequencies with respect to our method is lower than 0.6%. Moreover, it can be noticed, that the shift of the

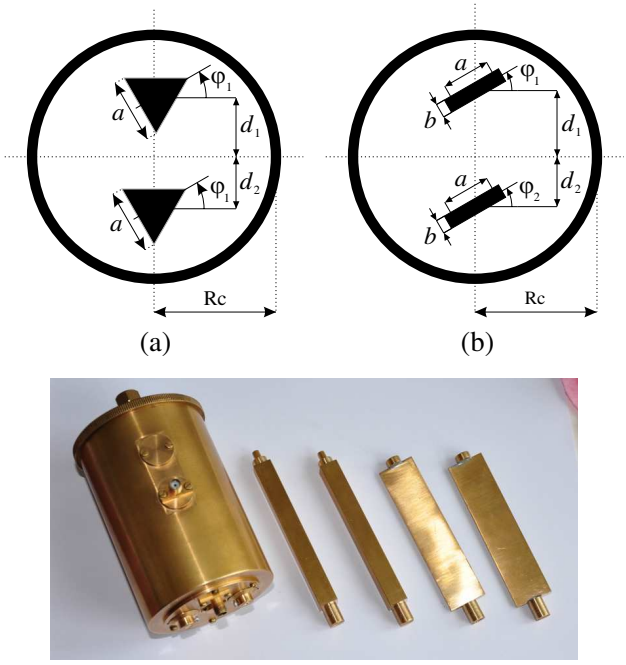

Figure 9. Schematic view of circular cavity resonator loaded with two (a) triangular and (b) rectangular symmetrically located posts and (c) photo of the fabricated structure.

post influences the resonant frequencies of the investigated resonator. When the distance d is decreased to 0 (centrally located post case), as one expects, the degenerate modes in the structure appears.

The next investigated structure is a resonator with two symmetrically located triangular posts which is schematically presented in Fig. 9(a).

The simulated and measured resonance frequencies of this structure are presented in Table 4. In the analysis of this structure the number of modes $M = 10$, mesh density $\mathrm{W} = 60 \times 180$ and $P = 20$ iterations in ISP were used. It can be noticed, that the measured results are in a good agreement with the results of simulation. The accuracy is higher than 0.6%. Moreover, a good agreement between our method results and the ones obtained from commercial software QuickWave is observed.

The last investigated structure is circular cavity resonator loaded with two rectangular posts. In the analysis of this structure the following parameters were assumed: Number of modes $M = 10$, mesh

Table 4. TM/TE-modes resonance frequencies (in GHz) for structure from Fig. 9(a) ($a = 11.5\,\mathrm{mm}$, $R = 30\,\mathrm{mm}$, $H = 86\,\mathrm{mm}$, $d = 15\,\mathrm{mm}$, $\varphi_1 = \varphi_2 = 0$).

n	Mode	Measurment	QW	err [%]	Our Method	err [%]
0	TM	5.685	5.6926	0.13	5.6982	0.23
	TM	6.378	6.4102	0.50	6.416	0.60
1	TE	3.182	3.1926	0.33	3.199	0.53
	TE	3.33	3.3406	0.32	3.3445	0.44
	TE	4.829	4.8447	0.33	4.8387	0.20
	TE	4.9	4.9119	0.24	4.925	0.51
	TM	5.958	5.9533	0.08	5.9597	0.03
	TE	5.972	5.987	0.25	6.0002	0.47
2	TE	4.39	4.3911	0.03	4.395	0.11
	TE	4.501	4.4999	0.02	4.505	0.09
	TE	5.699	5.7062	0.13	5.7159	0.30
	TE	5.76	5.7632	0.06	5.7767	0.29
3	TE	5.88	5.8625	0.30	5.878	0.03
	TE	5.94	5.9445	0.08	5.958	0.30

density $W = 40 \times 120$, and number of iterations $P = 20$. As in previous example a good agreement of simulated and measured results was obtained. The error between simulated and measured data is lower than 0.5%.

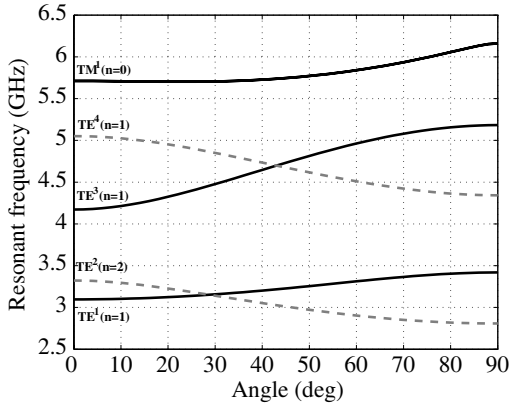

Figure 10. Resonant frequencies of the resonator loaded with two symmetrically located rectangular posts in function of posts rotation φ_1 and φ_2 ($a = 19.87\,\text{mm}$, $b = 2.95\,\text{mm}$, $R = 30\,\text{mm}$, $H = 86\,\text{mm}$, $d = 15\,\text{mm}$).

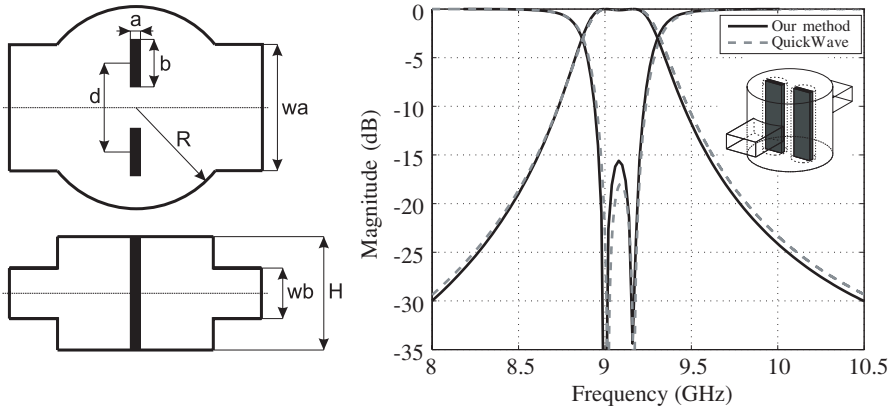

Figure 11. Circular cavity resonator loaded with asymmetrically located dielectric post and coupled with rectangular waveguides: (a) Dimension of the structure: $R = 20\,\text{mm}$, $H = 16.2\,\text{mm}$, $a = 1\,\text{mm}$, $b = 7\,\text{mm}$, $w_a = 22.86\,\text{mm}$, $w_b = 1.2\,\text{mm}$, (b) frequency response.

Additionally, for analyzed structure the influence of rotation of posts on resonance frequencies was investigated and the obtained results are presented in Fig. 10. It can be noticed that the rotation of posts allows one to change resonant frequencies in wide range. Moreover, for some angles of posts rotation the resonance frequencies of resonators become equal. The aforementioned properties of arbitrary cross section posts can be used in realization of tunable resonators and waveguide filters.

For the analyzed structures presented in Fig. 9, besides the TE/TM-modes the TEM-modes also appears as a solution of presented method. The resonance frequencies of these modes calculated from our method were the same as the ones obtained from analytical formula

$$f_0 = \frac{nc}{2H}, \qquad \text{where} \quad n = 1, 2, \ldots, N. \tag{24}$$

Table 5. TM/TE-modes resonance frequencies (in GHz) for structure from Fig. 9(b) ($a = 19.87\,\text{mm}$, $b = 2.95\,\text{mm}$, $R = 30\,\text{mm}$, $H = 86\,\text{mm}$, $d = 15\,\text{mm}$, $\varphi_1 = \varphi_2 = 0$).

n	Mode	Measurment	QW	err [%]	Our Method	err [%]
0	TM	5.703	5.711	0.15	5.712	0.16
	TM	6.78	6.819	0.57	6.812	0.47
1	TE	3.080	3.089	0.31	3.093	0.44
	TE	3.313	3.32	0.23	3.322	0.28
	TE	4.158	4.154	0.09	4.164	0.16
	TE	5.028	5.048	0.41	5.050	0.46
	TE	5.68	5.699	0.34	5.705	0.44
	TE	6.238	6.218	0.32	6.228	0.17
	TM	5.955	5.971	0.27	5.964	0.16
2	TE	4.316	4.318	0.05	4.322	0.15
	TE	4.488	4.486	0.04	4.489	0.03
	TE	5.13	5.133	0.06	5.143	0.26
	TE	5.868	5.881	0.23	5.884	0.28
3	TE	5.804	5.812	0.13	5.820	0.28
	TE	5.955	5.938	0.29	5.945	0.17

4.3. Waveguide Coupled Resonators

The investigated structure presented in Fig. 11(a) is consisted of circular cavity resonator loaded with two symmetrically located rectangular metalic posts and coupled with rectangular waveguides. The scattering parameters of this structure are presented in Fig. 11(b). In the scattering parameters calculation the mesh density $W = 40 \times 120$, number of cylindrical modes $M = 10$ and $N = 2$, number of iteration $P = 20$ was used in the cylindrical region. The obtained results are compared with commercial software QuickWave and a good agreement is achieved. It was observed that inserting the metallic post in the circular cavity resonator structure results in the shift of the resonant frequency of TM mode with $m = 0$ angular field variation close to the TM mode with $m = 1$ angular field variation. As a result, when circular cavity coupled resonator with rectangular waveguides is considered, a second order filter structure is obtained.

5. CONCLUSION

In this paper the new hybrid method based on a combination of mode-matching technique and finite difference frequency domain method is presented. In the analysis of multiple object structures the ISP procedure is used. The accuracy of method is presented. To verify the validity of our approach some numerical examples are considered. The results are compared with the results published in literature and the ones obtained from commercial software and own measurements. A good agreement of presented approach with other techniques and measured data is achieved.

ACKNOWLEDGMENT

This work was supported in part by the Polish State Committee for Scientific Research under Contract N515 418434.

APPENDIX A.

In Chapter 2.1, the following matrices takes the form:

$$\mathbf{M}_k^E = \operatorname{diag}\left(\mathbf{M}_{k,n}^E\right)_{n=0}^{n=N} \text{ where } \mathbf{M}_{k,n}^E = \begin{bmatrix} \mathbf{M}_{z,k,n}^{E^{(TM)}} & 0 \\ \mathbf{M}_{\varphi,k,n}^{E^{(TM)}} & \mathbf{M}_{\varphi,k,n}^{E^{(TE)}} \end{bmatrix},$$

and

$$\mathbf{M}_{z,k,n}^{E^{II(TM)}} = \mathrm{diag}(R_m^k(k_{\rho n}R))_{m=-M}^{m=M}, \text{ for } n = 0, \ldots, N$$

$$\mathbf{M}_{\varphi,k,n}^{E^{II(TM)}} = \mathrm{diag}\left(\frac{-jmk_{zn}}{k_{\rho n}^2 R} R_m^k(k_{\rho n}R)\right)_{m=-M}^{m=M},$$

$$\mathbf{M}_{\varphi,k,n}^{E^{II(TE)}} = \mathrm{diag}\left(\frac{j\omega\mu_0\mu_r}{k_{\rho n}^2} R_m'^k(k_{\rho n}R)\right)_{m=-M}^{m=M}, \text{ for } n = 1, \ldots, N$$

$$\mathbf{M}_k^{H^{II}} = \mathrm{diag}\left(\mathbf{M}_{k,n}^{H^{II}}\right)_{n=0}^{n=N} \text{ where } \mathbf{M}_{k,n}^{H^{II}} = \begin{bmatrix} \mathbf{M}_{\varphi,k,n}^{H^{II(TM)}} & \mathbf{M}_{\varphi,k,n}^{H^{II(TE)}} \\ 0 & \mathbf{M}_{z,k,n}^{H^{II(TE)}} \end{bmatrix},$$

and

$$\mathbf{M}_{z,k,n}^{H^{II(TM)}} = \mathrm{diag}(R_m^k k_{\rho n}R)_{m=-M}^{m=M},$$

$$\mathbf{M}_{\varphi,k,n}^{H^{II(TM)}} = \mathrm{diag}\left(\frac{-j\omega\varepsilon_0\varepsilon_r}{k_{\rho n}^2} R_m'^k(k_{\rho n}R)\right)_{m=-M}^{m=M} \text{ for } n = 1, \ldots, N,$$

$$\mathbf{M}_{\varphi,k,n}^{H^{II(TE)}} = \mathrm{diag}\left(\frac{jmk_{zn}}{k_{\rho n}^2 R} R_m^k(k_{\rho n}R)\right)_{m=-M}^{m=M} \text{ for } n = 0, \ldots, N,$$

APPENDIX B.

In Chapter 2.2 the matrices of space discretization in the ρ and φ direction, respectively, are expressed as follows:

$$\begin{aligned} \mathbf{D}_1 &= \mathrm{diag}\left[\Delta_\rho \mathbf{I}_{(W\times W)}, \Delta_\varphi \mathbf{I}_{(W\times W)}, \mathbf{I}_{(W+1\times W+1)}\right], \\ \mathbf{D}_2 &= \mathrm{diag}\left[\Delta_\rho \mathbf{I}_{(W\times W)}, \Delta_\varphi \mathbf{I}_{(W\times W)}, \mathbf{I}_{(W\times W)}\right], \\ \mathbf{S}_1 &= \mathrm{diag}\left[\Delta_\varphi \mathbf{I}_{(W\times W)}, \Delta_\rho \mathbf{I}_{(W\times W)}, \Delta_\rho\Delta_\varphi \mathbf{I}_{(W+1\times W+1)}\right], \\ \mathbf{S}_2 &= \mathrm{diag}\left[\Delta_\varphi \mathbf{I}_{(W\times W)}, \Delta_\rho \mathbf{I}_{(W\times W)}, \Delta_\rho\Delta_\varphi \mathbf{I}_{(W\times W)}\right], \end{aligned}$$

where $\Delta_\rho = R/V$, $\Delta_\varphi = 2\pi/K$ and the unit matrix of size $(n)\times(n)$ is denoted as: $\mathbf{I}_{(n\times n)}$. The matrices of the derivatives take the following form:

$$\mathbf{P}_1 = \begin{bmatrix} 0 & \mathbf{K}_z & -\mathbf{R}_{e1}\mathbf{P}_{\varphi 1} \\ -\mathbf{K}_z & 0 & \mathbf{P}_{\rho 1} \\ \mathbf{R}_h\mathbf{P}_\varphi & -\mathbf{R}_h\mathbf{P}_\varphi\mathbf{R}_e & 0 \end{bmatrix},$$

$$\mathbf{P}_2 = \begin{bmatrix} 0 & \mathbf{K}_z & \mathbf{R}_h\mathbf{P}_{\varphi 2} \\ -\mathbf{K}_z & 0 & -\mathbf{P}_{\rho 2} \\ -\mathbf{R}_{e2}\mathbf{P}_{\varphi} & \mathbf{R}_{e2}\mathbf{P}_{\varphi}\mathbf{R}_e & 0 \end{bmatrix},$$

where $\mathbf{K}_z = [k_{zn}\mathbf{I}_{W\times W}]$ and k_{zn} is a wavenumber along z-axis,

$$[\mathbf{P}_{\rho 1}]_{m,n} = \begin{cases} 1 & n = m+1, \\ -1 & (m \le K \wedge n = 1) \vee (m > K \wedge n = m-K), \\ 0 & \text{otherwise}, \end{cases}$$

$$[\mathbf{P}_{\varphi 1}]_{m,n} = \begin{cases} 1 & (n = m+1) \vee (m \mod K = 0 \wedge n = m-K), \\ -1 & (m \mod K \neq 0) \wedge (n = m), \\ 0 & \text{otherwise}, \end{cases}$$

for $m = 1, \ldots, W$ and $n = 1, \ldots, W+1$,

$$[\mathbf{P}_{\rho 2}]_{m,n} = \begin{cases} 1 & n = m+K, \\ -1 & n = m, \\ 0 & \text{otherwise}, \end{cases}$$

$$[\mathbf{P}_{\varphi 2}]_{m,n} = \begin{cases} 1/(0.5\pi\Delta_\rho) & (m = 1) \wedge (n = 1, \ldots, K), \\ 1 & (m = 2 \ldots N) \wedge (n = m), \\ -1 & (m = 2 \ldots N+1) \wedge (n = m-1), \\ 0 & \text{otherwise}, \end{cases}$$

for $m = 1, \ldots, W+1$ and $n = 1, \ldots, W$.

The matrices of the projection are expressed as follows:

$$[\mathbf{Q}_b]_{m,n} = \begin{cases} 1 & m = n, \\ 0 & \text{otherwise}, \end{cases}$$

for $m = 1, \ldots, W+1$ and $n = 1, \ldots, K$,

$$[\mathbf{Q}]_{m,n} = \begin{cases} 1 & m - K + 1 = n, \\ 0 & \text{otherwise}, \end{cases} \tag{B1}$$

and the matrices of the metric coefficients take the following form:

$$\mathbf{R}_{e1} = \operatorname{diag}\left[\rho_{e_{(1)}}, \ldots, \rho_{e_{(W)}}\right],$$

$$\mathbf{R}_{e2} = \operatorname{diag}\left[0, \rho_{e_{(1)}}, \ldots, \rho_{e_{(W)}}\right],$$

$$\mathbf{R}_{h} = \operatorname{diag}\left[\rho_{h_{(1)}}, \ldots, \rho_{h_{(W)}}\right].$$

The matrices of field expansion coefficients in Eq. (22) takes the following form:

$$C^E = \operatorname{diag}\left(C_0^{Ez}, C_1^{Ez}, C_1^{E\varphi}, \ldots, C_N^{Ez}, C_N^{E\varphi}\right)$$

$$\text{where} \quad C_n^{Ez(\varphi)} = \text{diag}\left(C_{n,-M}^{Ez(\varphi)}, \ldots, C_{n,M}^{Ez(\varphi)}\right)$$

$$\text{and} \quad D^H = \left[D_0^{H\varphi}, D_1^{H\varphi}, D_1^{Hz}, \ldots, D_N^{H\varphi}, D_N^{Hz}\right]$$

$$\text{where} \quad D_n^{H\varphi(z)} = \left[D_{n,-M}^{H\varphi(z)}, \ldots, D_{n,M}^{H\varphi(z)}\right]$$

$$\text{and} \quad D_{n,M}^{H\varphi(z)} = \left[D_{n,M,-M}^{H\varphi(z)}, \ldots, D_{n,M,M}^{H\varphi(z)}\right]^T.$$

REFERENCES

1. Satoh, T., S. Endo, N. Matsunaka, S. Betsudan, T. Katagi, and T. Ebisui, "Sidelobe level reduction by improvement of strut shape," *IEEE Trans. on AP*, Vol. 32, 698–705, Jul. 1984.
2. Kildal, P.-S., A. A. Kishk, and A. Tengs, "Reduction of forward scattering from cylindrical objects using hard surfaces," *IEEE Trans. on AP*, Vol. 44, 1509–1520, Nov. 1996.
3. Yasumoto, K., H. Toyama, and T. Kushta, "Accurate analysis of two-dimensional electromagnetic scattering from multilayered periodic arrays of circular cylinders using lattice sums technique," *IEEE Trans. on AP*, Vol. 52, 2603–2611, Oct. 2004.
4. Toyama, H. and K. Yasumoto, "Electromagnetic scattering from periodic arrays of composite circular cylinder with internal cylindrical scatterers," *Progress In Electromagnetics Research*, PIER 52, 321–333, 2005.
5. Gimeno, B., J. L. Cruz, E. A. Navarro, and V. Such, "A polarizer rotator system for three-dimensional oblique incidence," *IEEE Trans. on AP*, Vol. 42, No. 7, 912–919, Jul. 1994.
6. Lech, R., M. Mazur, and J. Mazur, "Analysis and design of a polarizer rotator system," *IEEE Trans. on AP*, Vol. 56, No. 3, 844–847, Mar. 2008.
7. Coccioli, R., A. Morini, G. Pelosi, and T. Rozzi, "Design of tolerance-corrected filters employing half-cylinder posts," *IEEE Trans. on MTT*, Vol. 46, No. 1, 116–118, Jan. 1998.
8. Bachiller, C., H. Esteban, V. E. Boria, J. V. Morro, L. J. Rogla, M. Taroncher, and A. Belenguer, "Efficient CAD tool of direct-coupled-cavities filters with dielectric resonators," *IEEE Antennas and Propagation Society International Symposium 2005*, Vol. 1B, 578–581, 2005.
9. Shen, T., K. A. Zaki, and C. Wang, "Tunable dielectric resonators with dielectric tuning disks," *IEEE Trans. on MTT*, Vol. 48, No. 12, 2439–2445, Dec. 2000.

10. Dittloff, J., F. Arndt, and D. Grauerholz, "Optimum design of waveguide E-plane stub-loaded phase shifters," *IEEE Trans. on MTT*, Vol. 36, No. 3, 582–587, Mar. 1988.
11. Gaiewski, W. R., L. P. Dunleavy, and A. J. Castro, "Analysis and measurement of mode polarizers in square waveguide," *IEEE Trans. on MTT*, Vol. 45, No. 6, 997–1000, Jun. 1997.
12. Sabbagh, M. E. and K. Zaki, "Modeling of rectangular waveguide junctions containing cylindrical posts," *Progress In Electromagnetics Research*, PIER 33, 299–331, 2001.
13. Arena, D., M. Ludovico, G. Manara, and A. Monorchio, "Analysis of waveguide discontinuities using edge elements in a hybrid mode matching/finite elements approach," *IEEE MWCL*, Vol. 11, No. 9, 379–381, Sep. 2001.
14. Crino, V., M. Mongiardo, and C. Tomassoni, "Comparison between line and surface integral formulations of the hybrid mode-matching/two-dimensional finite element method: Research articles," *International Journal of Numerical Modelling: Electronic Networks, Devices and Fields*, Vol. 17, No. 6, 575–592, Nov. 2004.
15. Catina, V., F. Arndt, and J. Brandt, "Hybrid surface integral-equation/mode-matching method for the analysis of dielectric loaded waveguide filters of arbitrary shape," *IEEE Trans. on MTT*, Vol. 53, No. 11, 3562–3567, Nov. 2005.
16. Abd-Alhameed, R. A., P. S. Excell, M. A. Mangoud, and J. A. Vaul, "Computation of radiated and scattered field using separate frequency domain moment-method regions and frequency domain MoM-FDTD hybrid methods," *IEE Antennas and Propagation 1999 National Conference*, Vol. 30, Mar./Apr. 1999.
17. Rogier, H., "A new hybrid FDTD-BIE approach to model electromagnetic scattering problems," *IEEE Microwave and Guided Wave Letters*, Vol. 8, No. 3, 138–140, Mar. 1998.
18. Xu, F. and W. Hong, "Analysis of two dimensions sparse multicylinder scattering problem using DD-FDTD method," *IEEE Trans. on AP*, Vol. 52, No. 10, 2612–2617, Oct. 2004.
19. Sharkawy, M. A., V. Demir, and A. Z. Elsherbeni, "Plane wave scattering from three dimensional multiple objects using the iterative multiregion technique based on the FDFD method," *IEEE Trans. on AP*, Vol. 54, No. 2, 666–673, Feb. 2006.
20. Esteban, H., S. Cogollos, V. E. Boria, A. S. Blas, and M. Ferrando, "A new hybrid mode-matching/numerical method for the analysis of arbitrarily shaped inductive obstacles and discontinuities in rectangular waveguides," *IEEE Trans. on MTT*, Vol. 50, No. 4, 1219–1224, Apr. 2002.

21. Arndt, F., V. Catina, and J. Brandt, "Efficient hybrid MM/MoM technique for the CAD of circular combline filters with resonators of more general shape," *IEEE Microwave Symposium Digest*, Vol. 3, 1407–1410, 2004.
22. Polewski, M. and J. Mazur, "Scattering by an array of conducting lossy dielectric, ferrite and pseudochiral cylinders," *Progress In Electromagnetics Research*, PIER 38, 283–310, 2002.
23. Polewski, M., R. Lech, and J. Mazur, "Rigorous modal analysis of structures containing inhomogeneous dielectric cylinders," *IEEE Trans. on MTT*, Vol. 52, No. 5, 1508–1516, May 2004.
24. Kusiek, A., R. Lech, and J. Mazur, "A new hybrid method for analysis of scattering from arbitrary configuration of cylindrical objects," *IEEE Trans. on AP*, Vol. 56, No. 6, 1725–1733, Jun. 2008.
25. Quick Wave 3D, QWED, Warsaw, Poland, 2006.
26. Taflove, A., *The Finite-difference Time-domain Method*, Artech House, 1995.
27. Dey, S. and R. Mittra, "A conformal finite-difference time-domain technique for modeling cylindrical dielectric resonators," *IEEE Trans. on MTT*, Vol. 47, No. 9, 1737–1739, Sep. 1999.
28. Kaneda, N., B. Housmand, and T. Itoh, "FDTD analysis of dielectric resonators with curved surfaces," *IEEE Trans. on MTT*, Vol. 45, No. 9, 1645–1649, Sep. 1997.
29. Kowalczyk, P., M. Wiktor, and M. Mrozowski, "Efficient finite difference analysis of microstructured optical fibers," *Opt. Express*, Vol. 13, No. 25, 10349–10359, Dec. 2005.
30. Dahlquist, G. and A. Bjrck, *Numerical Methods,* Prentice Hall, 1974.
31. Kusiek, A., P. Kowalczyk, and J. Mazur, "Analysis of scattering from arbitrary configuration of elliptical obstacles using T-matrix representation," *IET Microwaves, Antennas and Propagation*, Vol. 2, No. 10, 434–441, Aug. 2008.
32. Tsalamengas, J. L., I. O. Vardiambasis, and J. G. Fikioris, "Plane-wave scattering by strip-loaded circular dielectric cylinders in the case of oblique incidence and arbitrary polarization," *IEEE Trans. on AP*, Vol. 43, No. 10, 1099–1108, Oct. 1995.